

THESIS FOR THE DEGREE OF LICENTIATE OF ENGINEERING

# Inverse modelling of GNSS multipath signals

A novel method for GNSS reflectometry

JOAKIM STRANDBERG

Department of Space, Earth and Environment  
Onsala Space Observatory  
CHALMERS UNIVERSITY OF TECHNOLOGY  
Gothenburg, Sweden 2017

Inverse modelling of GNSS multipath signals  
A novel method for GNSS reflectometry  
JOAKIM STRANDBERG

© JOAKIM STRANDBERG, 2017

Department of Space, Earth and Environment  
Onsala Space Observatory  
Chalmers University of Technology  
SE-412 96 Gothenburg  
Sweden  
Telephone: +46 (0)31-772 1000

Cover:  
Photography of the GTGU/GTGD dual antenna installation for GNSS reflectometry  
at the Onsala Space Observatory, Sweden.

Chalmers Reproservice  
Gothenburg, Sweden 2017

Inverse modelling of GNSS multipath signals  
A novel method for GNSS reflectometry  
JOAKIM STRANDBERG  
Department of Space, Earth and Environment  
Chalmers University of Technology

## Abstract

Measuring the world around us is necessary to observe and understand the changes that occur in our environment. A widely distributed network of measurement stations can help us to understand ongoing and predict future climate change. GNSS reflectometry has the capacity of providing data from all over the world, as there are already many GNSS stations established and operated for navigational and meteorological purposes. This thesis presents a new way of retrieving environmental data from GNSS signal-to-noise ratio measurements which has the capability to provide new types of measurements. The method is based on inverse modelling of the signal-to-noise ratio in order to retrieve physical parameters of reflecting surfaces around GNSS installations. It is successfully demonstrated that the method improves the precision of the GNSS reflectometry derived sea surface height measurements significantly. By using the signal-to-noise ratio pattern, it is also — for the first time — demonstrated that it is possible to use GNSS reflectometry to detect coastal sea ice.

Keywords: GNSS, reflectometry, sea level, sea ice



# Acknowledgements

This page has been the single largest cause of anxiety in the whole thesis. Facts are easy, people are not. There are just so many people that have influenced me throughout my life that it is impossible to mention you all. But still I would like to direct a special thanks to some persons that have been important throughout the process of producing this thesis.

Naturally, I would like to start with my main supervisor, Thomas Hobiger, who has provided me with many ideas and angles on different problems and have tirelessly read through and commented on drafts over and over again. I would also like to thank my co-supervisor and group leader, Rüdiger Haas, for feedback to papers and presentations. And to all other colleagues at the department, thank you for all the interesting discussions around the coffee table, at lunch, and in the space bus, which make the days more interesting.

To family and relatives, thanks for your support and encouragement, and for answering the continuous stream of “How?” and “Why?” that the 6-year old me asked. Thanks also to my closest friends for discussions about life in general and the PhD life in particular, and for the time spent in the pen-and-paper worlds.

Finally, music has always been important for me, especially as a way to relax however stressful everything else is. Therefore, I would like to direct a special thanks to everyone in Chalmersspexet Vera, Aspen Big Band, and at Lerums Kulturskola, for giving me a context in which to play music together with other wonderful people.

Joakim



# Research contributions

This thesis is based on the work contained in the following papers:

- I** J. Strandberg et al. (2016b). “Inverse modelling of GNSS multipath for sea level measurements - initial results”. *Proc. of International Geoscience and Remote Sensing Symposium 2016 (IGARSS 2016)*. DOI: 10.1109/IGARSS.2016.7729479
- II** J. Strandberg et al. (2016a). Improving GNSS-R sea level determination through inverse modeling of SNR data. *Radio Science*, **51**(8), 1286–1296. DOI: 10.1002/2016RS006057
- III** J. Strandberg et al. (2017). Coastal sea ice detection using ground-based GNSS-R. *IEEE Geoscience and Remote Sensing Letters*, in press.



# Nomenclature

$C_{i,1}, C_{i,2}$	In-phase and quadrature amplitudes of SNR oscillations
$\gamma$	Damping coefficient
$\lambda$	Wavelength
$k$	Wave number: $k = \frac{2\pi}{\lambda}$
$s$	Surface standard deviation
$\phi$	Interferometric phase delay
$\varphi$	Phase shift of the SNR oscillations
$\varepsilon, \dot{\varepsilon}$	Satellite elevation angle and its time derivative
$x$	Sine of elevation angle: $x = \sin \varepsilon$
$h, \dot{h}$	Reflector height and its time derivative
$P_d, P_r, P$	Direct, reflected and total received power at the antenna
$R^C, R^X$	Fresnel reflection for co- and cross-circularly polarised signals
$G^R, G^L$	Antenna gain for right and left hand circularly polarised signals
$\Phi^R, \Phi^L$	Phase delays from antenna patterns
$X$	Coupled antenna-surface vector
$S$	Coherence factor
$N_j$	B-spline nodes

## Abbreviations

GLONASS	Globalnaja Navigatsionnaja Sputnikovaja Sistema
GNSS	Global Navigation Satellite System
GNSS-MR	GNSS multipath reflectometry
GNSS-R	GNSS reflectometry
GPS	Global Positioning System
GTGU	GNSS Tide Gauge Up
GTGD	GNSS Tide Gauge Down
IGS	International GNSS Service
SMHI	Swedish Meteorological and Hydrological Institute
SNR	Signal-to-noise ratio
SSH	Sea surface height



# Contents

Abstract . . . . .	i
Acknowledgements . . . . .	iii
Research contributions . . . . .	v
Nomenclature . . . . .	vii
Contents . . . . .	ix
<b>1 Introduction</b>	<b>1</b>
1.1 Outline of the Thesis . . . . .	1
1.2 Global Navigation Satellite Systems . . . . .	1
1.3 GNSS Reflectometry in a Nutshell . . . . .	3
1.4 The GTGU Research Installation . . . . .	4
<b>2 GNSS Reflectometry</b>	<b>7</b>
2.1 Dedicated GNSS-R Instruments . . . . .	7
2.2 Interference Pattern Analysis . . . . .	8
2.3 Inverse Modelling . . . . .	12
2.3.1 Representing Height as Time Dependent B-spline . . . . .	16
2.3.2 Retrieval Procedure . . . . .	17
2.4 Applications of GNSS Reflectometry . . . . .	18
2.4.1 Sea Surface Height Measurements . . . . .	18
2.4.2 Ice Detection . . . . .	21
2.4.3 Snow Depth Measurements . . . . .	22
<b>3 Summary and Outlook</b>	<b>25</b>
<b>4 Summary of Appended Papers</b>	<b>27</b>
4.1 Summary of Paper I: Inverse modelling of GNSS multipath for sea level measurements - initial results . . . . .	27
4.2 Summary of Paper II: Improving GNSS-R sea level determination through inverse modelling of SNR data . . . . .	27
4.3 Summary of Paper III: Coastal sea ice detection using ground-based GNSS-R . . . . .	28
<b>Bibliography</b>	<b>29</b>
<b>Paper I</b>	<b>33</b>
<b>Paper II</b>	<b>39</b>
<b>Paper III</b>	<b>53</b>



# Chapter 1

## Introduction

Observing our environment is important for the understanding of changes that occur around us due to natural variations as well as anthropogenic influence. To be able to state that the climate has changed, climatologists require long time series to average out any short-term temporary fluctuations. Typically, the time series lengths should be at least on the order of many decades to be useful as credible evidence for any climate change.

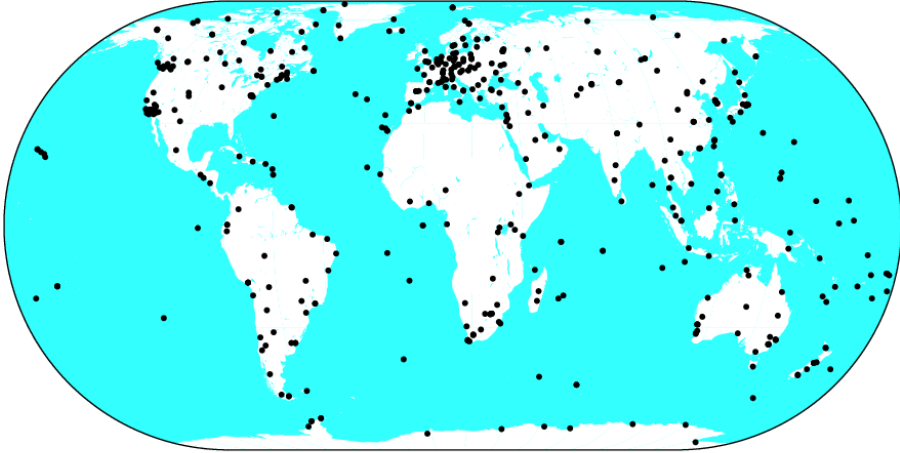
Among the scientists that rely on really long and stable time series are geodesists that study Earth's shape, rotational behaviour, and gravity field. They require multi-decade measurement series, with no change of equipment, in order to observe the slow motion of the crust. The field of GNSS reflectometry draws from both of these fields: using geodetic instruments to measure parameters with relevance to climate research.

### 1.1 Outline of the Thesis

The following parts of this chapter provide a short introduction to Global Navigation Satellite Systems (GNSS), and how one can benefit from using already existing systems for new research purposes. Chapter 2 explains the concept of GNSS reflectometry and introduces our new inverse model algorithm, Chapter 3 gives a very brief summary and outlook, and finally Chapter 4 introduces the papers on which this thesis is based. Chapter 1 is targeted towards a reader with an interest in science and technology, while Chapter 2 and onwards may require a basic background in engineering and/or physics.

### 1.2 Global Navigation Satellite Systems

Global Navigation Satellite Systems – GNSS for short – is a collective term for all satellite systems used for positioning, navigation, and timing. These satellite systems are used both for everyday purposes, such as positioning your phone or your car, but also for more precise applications, such as monitoring very small



IGS1 2016 Jun 29 17:01:00

Figure 1.1: *The International GNSS Service network (Dow et al., 2009) collects data from national networks around the world and distribute it publicly. Illustration taken from the IGS webpage<sup>1</sup>.*

changes and movements of the crust of Earth. They also play a crucial role in the internet infrastructure, by providing time references to users all around the world.

The term GNSS encompasses several satellite systems operated by different entities: the widely known **G**lobal **P**ositioning **S**ystem (GPS) which is operated by the US government, the Russian system **G**lobalnaja **N**avigatsionnaja **S**putnikovaja **S**istema (GLONASS), China's BeiDou system, and since recently the European constellation Galileo which is the only fully civilian system. In addition, there are two systems with only regional coverage over India and Japan, respectively. The various systems operates on slightly different principles, but common to all of them is that they consist of several satellites orbiting Earth while broadcasting their position and clock information. As a very simplified description, the systems are used by determining the distance to at least four satellites to estimate the position and time of a receiver. At least four measurements are needed as there is four unknowns: position in three dimensions and time.

Currently there are more than 70 satellites distributed among the four global GNSS systems, and at most locations around the world there are usually more than ten satellites in view unless buildings or other tall structures are obstructing the sky. This means that it is possible to determine the position of a receiver anywhere in the world. Each system broadcasts several signals on different frequencies. Some of the signals that are broadcast from the satellites are encrypted, but most are freely available and accessible to anyone.

Around the world there exist many permanent station networks, such as the network coordinated by the International GNSS Service (IGS) shown in Figure 1.1.

<sup>1</sup>[https://igsceb.jpl.nasa.gov/images/maps/all\\_world\\_clean.png](https://igsceb.jpl.nasa.gov/images/maps/all_world_clean.png), accessed 30 June 2016.



Figure 1.2: *The GTGU/GTGD research installation at the Onsala Space Observatory, Sweden, consisting of two permanently operating antenna/receiver pairs.*

Among other purposes, these are used to monitor the movement of the continents and to provide a common position reference for users around the globe. The data collected by these networks are often freely available for everyone. As such they constitute a very large open dataset for anyone to analyse.

### 1.3 GNSS Reflectometry in a Nutshell

The simplified description of the principle of GNSS is of course very idealistic. In reality, there are several different error sources that affect the measurements of the distances to the satellites, and that have to be accounted for with various approaches. However, as it turns out, one of these error sources is actually the signal that we use for GNSS reflectometry.

Central to the method presented in this thesis is that GNSS satellites transmit electromagnetic signals on radio frequencies. This means that these signals are reflected off most surfaces found in nature. Therefore, there is not only one copy of the signal that reaches the antenna; the antenna receives both the signals that come directly from the satellites, and also the signals that have been reflected, and both of them affect the receiver tracking.

In short, the idea is that since GNSS signals are affected by so called multipath – reflections from surfaces surrounding a receiver – the sum of the direct and the reflected signal contains information about the objects causing the multipath effect. This information can be used to measure for example sea surface height, soil



Figure 1.3: *The Super Mareograph at the Onsala Space Observatory. Inside the stilling well there are four instruments — two pressure sensors, one radar, and one laser — measuring the water level continuously. A third pressure sensor is mounted outside the well.*

moisture, ice coverage, and snow height, all of which will be described in more detail in the following chapters. Important is that the method discussed in this thesis uses unmodified commercially-of-the-shelf GNSS receivers, such as the ones used for plate tectonic studies or regional reference station networks. This means that GNSS stations that are constructed for different purposes can directly be used for GNSS reflectometry without modification. Together with the large number of GNSS stations with public data around the world, the technique provides us with a large dataset that can be analysed.

## 1.4 The GTGU Research Installation

The Onsala Space Observatory hosts a special GNSS installation built specifically for GNSS reflectometry (Löfgren et al., 2011b), see Figure 1.2. This installation is used as a test bed for water related GNSS reflectometry measurements under ideal and controllable conditions. The installation consists of two GNSS antennas mounted on a beam over the sea surface. This results in an ideal view of the water surface, with very few obstructions affecting the measurements. The antennas are also mounted with the sea to the south, and as they are situated on the west coast of Sweden at  $57^{\circ}\text{N}$ , most satellite passages occur to the south, i.e. over the water surface. The two antennas are mounted so that one is pointing upward, named

GTGU, and the other one straight down, named GTGD. They are also sensitive to different polarisations, where the upward facing antenna is sensitive to right-hand circular polarisation, and the downward looking antenna is sensitive to left-hand circular polarisation. As the signal from the satellites are predominantly right-hand circularly polarised, this configuration makes GTGU sensitive to direct signals, and GTGD to reflected signals which change their polarisation in the reflection.

Close to the GTGU/GTGD installation, there is a traditional high precision tide gauge (Figure 1.3), measuring the sea level inside a stilling well. This tide gauge is part of the sea level monitoring network of the Swedish Meteorological and Hydrological Institute (SMHI) and can be used as a reference which allow us to evaluate the precision of GNSS reflectometry algorithms.

From measurements with the tide gauge we know that the tides at Onsala are moderate. Typically the tidal variation is around 20 cm to 30 cm. However, local weather conditions, such as pressure and wind, are the dominant effects at the location and can cause additional vertical sea surface displacements from 1 m below to 2 m above the mean sea level.



## Chapter 2

# GNSS Reflectometry

The field of GNSS reflectometry started in 1993 under the concept name of PARIS, *A Passive Reflectometry and Interferometry System* (Martin-Neira, 1993). At the time it was only used to describe GNSS-R observations from satellite platforms for ocean altimetry and for ocean wind determination (Garrison et al., 1998). Later on, ground-based applications for GNSS reflectometry were explored under two main concepts, either by measuring time of flight differences for the direct and reflected signal with dedicated hardware (Fabra et al., 2012; Martin-Neira et al., 2002) or by observing the effect of multipath on the signal-to-noise ratio using only an unmodified antenna and receiver (Anderson, 2000; Larson et al., 2008a). The work in this thesis is focused on the latter concept which will be described in detail in this chapter. However, for completeness and comparison, the conceptually simpler method using dedicated hardware will also be introduced.

### 2.1 Dedicated GNSS-R Instruments

GNSS receivers determine their main observable, the pseudo-range to the satellite, by correlating the received signal to a locally generated copy of the transmitted code to determine the delay between transmission and reception, i.e. the time of flight. In dedicated GNSS-R instruments, the replica code is also correlated against the reflected signal. This can be achieved in two ways: if the antenna is mounted sufficiently high the delay between the direct and reflected signal is large enough that both signals can be clearly distinguished using a purposefully built receiver (Martin-Neira et al., 2001). Or if two antennas are used, one of them can be designed to be sensitive to the direct signals and the other to the reflected signals (Martin-Neira et al., 2002). Of these two methods, the latter is the more common as it allows operation at low antenna heights, even down to a few meters. In that configuration there is one antenna pointing toward zenith that is susceptible for right hand circularly polarised signals, and a tilted antenna susceptible to left hand polarisation.

By comparing the time of flight of the direct and reflected signals the path delay is retrieved. To couple this path delay to a reflector height is then just pure

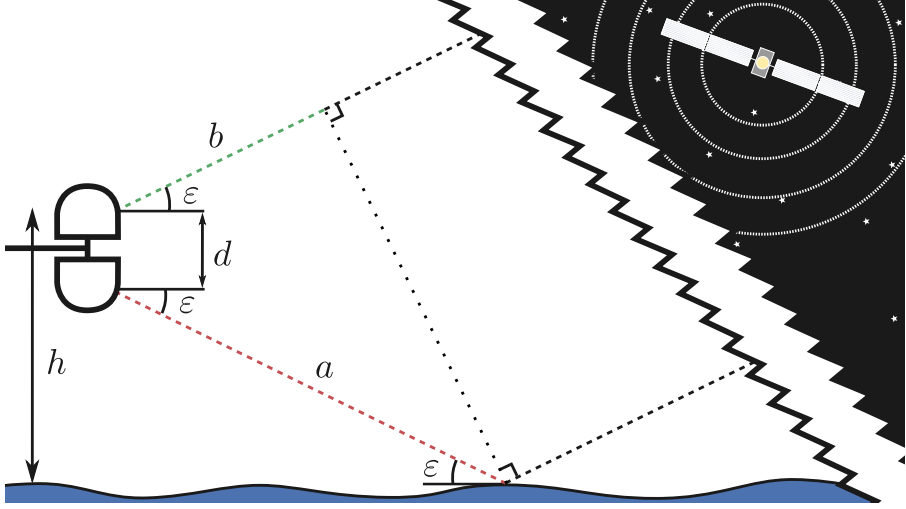


Figure 2.1: *Schematic drawing of the installation required for phase delay measurements. Because of the distance to the satellites relative to the reflector height, the incident wave can be assumed planar at the receiver.*

geometry. Referring to Figure 2.1 for the notation, the height  $h$  can be retrieved as:

$$h = \frac{1}{2} \left( \frac{a - b}{\sin \varepsilon} + d \right), \quad (2.1)$$

where  $a - b$  is simply the measured path difference between the two signals.

The method requires that both the zenith-looking and the nadir-looking antenna-receiver pairs are able to lock on to the transmitting GNSS satellites. If the sea surface becomes too rough, for example because of wind conditions, the nadir looking system can lose track of the satellite signals (Löfgren et al., 2011a), which is a major drawback for the technique in non-optimal locations.

## 2.2 Interference Pattern Analysis

In contrast to the dedicated GNSS-R measurements, the technique varyingly called GNSS multipath reflectometry (GNSS-MR) or interference pattern analysis relies only on one commercially-off-the-shelf GNSS receiver using the data it collects in standard operation. In addition to information about the distance to a specific satellite, commercial receivers are also able to record the signal-to-noise ratio (SNR), which is roughly proportional to the signal power. Because of coherent reflections, the direct and reflected signals are added according to the phasor diagram presented in Figure 2.2.  $V_d$  and  $V_r$  are the complex voltages of the two signals, and  $V$  the complex voltage of the combination. Since the power is proportional to the square of the voltage,  $P = V^2$ , the composite power of the direct and the reflected signals

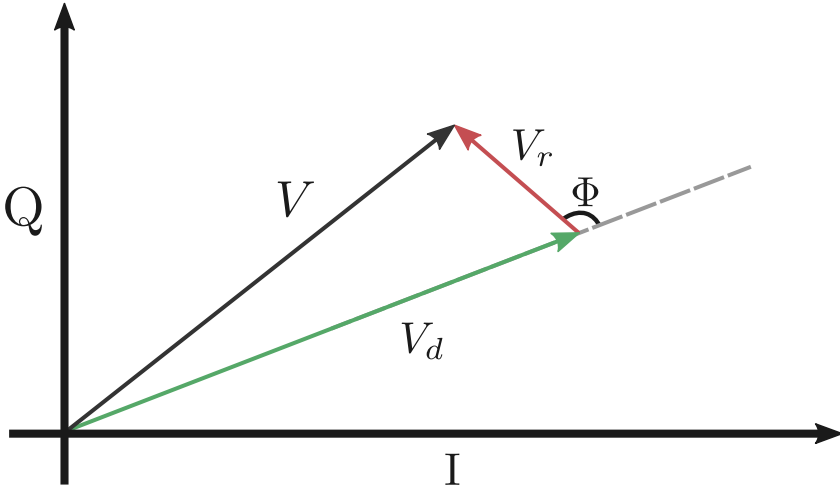


Figure 2.2: *Phasor diagram for the combination of the direct and reflected signal, where  $V_d$  and  $V_r$  are their respective complex voltages, and  $V$  is the voltage of the combined signal.  $I$  and  $Q$  refers to the in-phase and quadrature channels of the GNSS tracking loop.*

becomes (Georgiadou and Kleusberg, 1988)

$$P = P_d + P_r + 2\sqrt{P_r P_d} \cos(\phi), \quad (2.2)$$

where the subscripts  $r$  and  $d$  denotes reflected and direct signals respectively.  $\phi$  is the interferometric phase, i.e. the phase delay between the two signals. Intuitively this will depend on geometry as longer excess path means larger phase delay, but dielectric properties of the reflector will also affect the phase difference.

Generally, the extra path length travelled by the reflected signal can be described for an antenna mounted above a flat, tilted plane as

$$\tau = 2h' \sin(\varepsilon - \alpha) = 2h \frac{\sin(\varepsilon - \alpha)}{\cos \alpha}. \quad (2.3)$$

In the equation,  $h$  is the vertical distance from the antenna to the plane,  $\alpha$  is the plane tilt angle, and  $\varepsilon$  is the satellite elevation angle as depicted in Figure 2.3. However, a common assumption in GNSS reflectometry is that the reflecting surface is horizontal, i.e.  $\alpha = 0$ . This is usually a good assumption for sea surfaces, at least locally, and works for many land applications over for example crop fields as well (Larson et al., 2008b). The assumption of horizontal reflectors reduces Equation (2.3) to

$$\tau = 2h \sin \varepsilon. \quad (2.4)$$

The phase delay depends on the wavelength of the signal, and can be written as

$$\phi = \frac{2\pi}{\lambda} \tau. \quad (2.5)$$

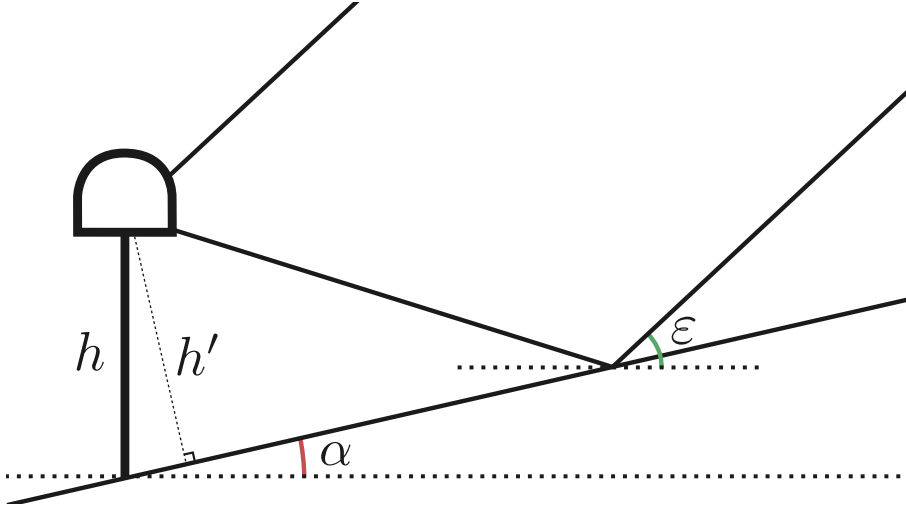


Figure 2.3: Schematic drawing for the interference pattern analysis with a tilted reflector. Both  $\alpha$  and  $\varepsilon$  are considered positive if the slope is positive with increasing distance from the antenna.

Thus the total interferometric phase becomes

$$\phi = \frac{4\pi h}{\lambda} \sin \varepsilon + \varphi, \quad (2.6)$$

where  $\varphi$  has been added to account for material properties of the reflector that can cause additional non-geometric phase delays. By combining Equations (2.2) and (2.6), it is evident that the signal-to-noise ratio, which is defined as received power over noise power, will contain information about the position of the reflector in relation to the antenna.

To extract the interesting information out of the raw signal-to-noise ratio data, it is often divided into two components,  $\text{SNR}_t$  and  $\delta\text{SNR}$ , i.e.

$$\text{SNR} = \text{SNR}_t + \delta\text{SNR}. \quad (2.7)$$

The first term describes a long period trend, as a result of the antenna gain pattern and atmospheric attenuation, and thus contains no information about the reflector. The  $\delta\text{SNR}$  component on the other hand comes from the oscillating part of Equation (2.2) which depends on the reflector. Therefore the signal-to-noise ratio can be detrended using a low degree polynomial to remove the influence of  $\text{SNR}_t$  and to focus only on the information carried in the oscillations. Both the oscillatory behaviour and the trend of the signal-to-noise ratio are shown in Figure 2.4.

After the signal has been detrended, only the oscillating part  $\delta\text{SNR}$  remains. From Equation (2.6), it is clear that the oscillations contain information about the reflector height. We can differentiate the interferometric phase in Equation (2.6)

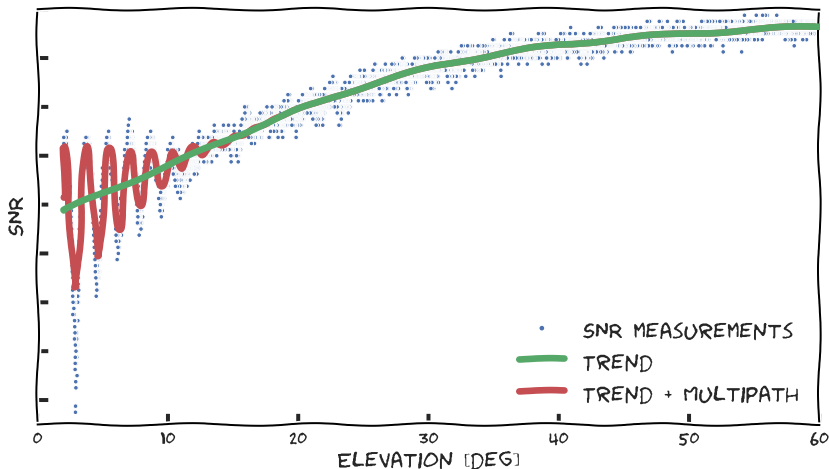


Figure 2.4: *The signal-to-noise ratio consist of an overall trend and the superimposed multipath interference. The data shown here was collected during an arbitrary satellite passage at GTGU at the Onsala Space Observatory, Sweden*

with respect to  $\sin \varepsilon$  to obtain

$$\frac{\partial \phi}{\partial \sin \varepsilon} = \frac{4\pi h}{\lambda}. \quad (2.8)$$

This means that the frequency of the oscillations with elevation, or rather with respect to the sine of elevation, is directly dependent on the reflector height. Thus, in a  $\sin \varepsilon$ -spectra of  $\delta\text{SNR}$ , there will be a clear peak corresponding to the vertical distance to the surface, assuming that the signal is only affected by a single horizontal multipath source.

Because the signal becomes unevenly sampled in  $\sin \varepsilon$ , standard Fourier transform algorithms do not work without applying techniques such as re-sampling, which tend to create artificial fringes. Instead, Lomb-Scargle analysis is commonly used to retrieve the power spectrum. Figure 2.5 shows two such spectra for different times of the same day, where the frequencies have already been converted to reflector heights. In the time between the two spectra the sea surface increased by about 35 cm according to a nearby tide gauge, which corresponds roughly to the observed frequency shift respectively height.

In the derivation of Equation (2.8), several assumptions are made. Most importantly that the height is constant during the period of the analysed satellite passage. For sufficiently small tidal variations, or for semi-static applications such as snow height measurements, the assumption does not affect the retrieved reflector height very much. However, for example at coastal locations with large variations of the sea surface height, the change of height will have a non-negligible effect (Larson et al., 2013). Instead of the oscillation frequency in Equation (2.8), we

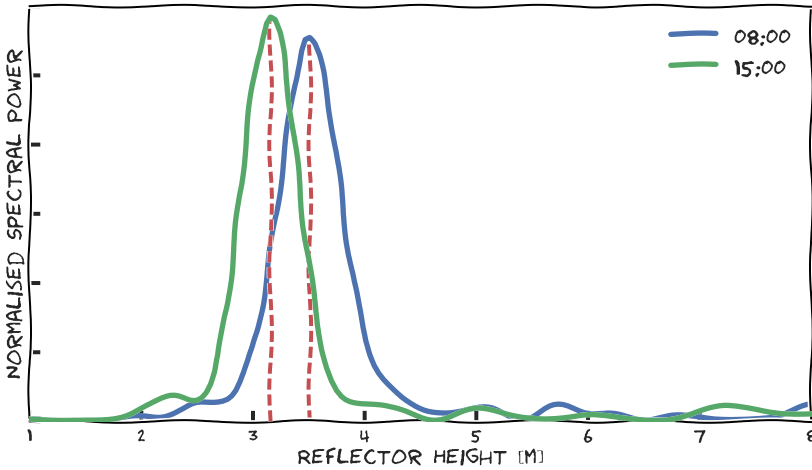


Figure 2.5: *Two Lomb-Scargle power spectra from GTGU in Onsala, at Dec. 23, 2015. The nearby tide gauge reports a difference of roughly 35 cm between the two measurements.*

introduce  $h \rightarrow h(t)$  and obtain

$$\frac{\partial \phi}{\partial \sin \varepsilon} = \frac{\partial \phi}{\partial t} \frac{\partial t}{\partial \sin \varepsilon} = \frac{4\pi h}{\lambda} + \frac{4\pi \dot{h} \tan \varepsilon}{\lambda \dot{\varepsilon}}, \quad (2.9)$$

where  $\dot{\varepsilon}$  and  $\dot{h}$  are the time derivatives of the reflector height and the satellite elevation respectively. Of these,  $\dot{\varepsilon}$  is a known value, since the satellite orbits are known to a sufficient accuracy. However,  $\dot{h}$  is unknown. This means that the reflector height cannot be directly retrieved from the power spectra, as the equation contains two unknowns. The problem is solved by noting that the first term in Equation (2.9) is the same term as in Equation (2.8). Therefore, the height and change rate is retrieved iteratively by first calculating the reflector heights under the assumption of a static reflector, then using the calculated heights to estimate the change rate which in turn is used to correct the retrieved heights (Larson et al., 2013; Löfgren et al., 2014).

### 2.3 Inverse Modelling

The new method presented in this thesis is based on the interference pattern method, i.e. using the oscillating part of the signal-to-noise ratio as the input data. But instead of using spectral analysis to retrieve reflector height we apply inverse modelling. To motivate the method we start by noticing that the Lomb-Scargle analysis focuses solely on the interferometric phase of the signal-to-noise ratio, treating the oscillations as pure sine waves. However, from Figure 2.4, it is evident that other elevation dependent effects are involved since the oscillations disappear



Figure 2.6: *Specular reflections are visible for example when the sun is near the horizon, as in this photo from the harbour of Vrångö, Sweden. The dependence of the diffusive scattering on the roughness can also be seen in the photo.*

above a certain elevation. The amplitude depends on the received reflected power, i.e.  $P_r$  in Equation (2.2). According to Nievinski and Larson (2014b), this term can be written as

$$P_r = P_d |X|^2 S^2. \quad (2.10)$$

As before,  $P_d$  is the direct incident power.  $X$  is a complex vector describing the effects of both the antenna and the reflector, and  $S$  represents the loss of coherence from scattering on a rough surface.

The scatter of a radio signal on a surface can be divided into specular reflection and diffuse scattering. Specular reflections can be compared to mirror reflections, i.e. a reflection that retains all information of the incident signal. Diffuse scattering, on the other hand, are reflections in which the coherency of the signal is lost. As GNSS reflectometry requires a coherent reflected signal for interference with the direct signal, only the specular reflections contribute to the retrieved information.

According to Beckmann and Spizzichino (1987), the loss of coherence from reflections on a horizontal surface with some roughness can be described as  $P_{\text{coherent}} = S^2 P_{\text{incident}}$ , where

$$S = \exp(-4k^2 s^2 \sin^2 \varepsilon). \quad (2.11)$$

Here we have used the wave number  $k = 2\pi/\lambda$  for brevity. The roughness of the surface is parametrised by the standard deviation  $s$  of its surface height. In coastal applications this would typically be the roughness caused by wind driven waves.

From Equation (2.11) it can be noted that the coherence of the reflected signal decreases with elevation, i.e. multipath interference is most prominent at low elevations. This is the same behaviour as seen in Figure 2.4 where the oscillations disappear when the satellite rises above about  $15^\circ$  elevation.

The middle term of Equation (2.10),  $X$ , considers both the directional dependency of the antenna gain as well as dielectric properties of the reflecting surface. More specifically it depends on the elevation dependent Fresnel reflection coefficients. Assuming a purely right hand circularly polarised incident wave,  $X$  can be rewritten as (Nievinski and Larson, 2014b)

$$X = R^C \sqrt{G^R} \exp(i\Phi^R) + R^X \sqrt{G^L} \exp(i\Phi^L). \quad (2.12)$$

$R^C$  and  $R^X$  are the co- and cross-circular Fresnel reflection coefficients,  $G^R$  and  $G^L$  the antenna gain for the two circular polarisations, and  $\Phi^R$  and  $\Phi^L$  the phase delays caused by the antenna. Therefore, due to the depolarisation caused by the reflection, the effects of the antenna and the surface will be mixed and inseparable even if the incident wave is purely right hand circularly polarised. To accurately model  $X$  the antenna gain pattern must be known for the specific antenna configuration. As this can vary significantly between different installations, and accurate antenna gain patterns are not available for all stations, the effect will not be explicitly modelled in the following, implicitly assuming  $X = 1$ . Therefore, care must be taken when interpreting any other elevation dependent effects, such as the coherence loss because of roughness.

Inserting the interferometric phase of Equation (2.6) and the expression for the reflected power in Equation (2.10) into Equation (2.2) gives the following expression for the oscillatory part of the signal-to-noise ratio:

$$\delta\text{SNR} = 2 P_d S \cos\left(\frac{4\pi h}{\lambda} \sin \varepsilon + \varphi\right), \quad (2.13)$$

where we, as previously mentioned, have omitted the effect of the Fresnel coefficients and the antenna gain. This formula is the basis for the inversion of GNSS signal-to-noise ratio data. The model is depicted together with measurements in Figure 2.7.

In order to be able to invert the  $\delta\text{SNR}$  observations more assumptions are necessary. First, we assume that the directly received power is constant over a whole inversion period, which follows from the constant power output from the GNSS satellites. Secondly, we have to make an assumption about the offset  $\varphi$ . This assumption will be different depending on environmental conditions, but for sea surface retrieval can assume that this property is also constant in time, as the phase offset is mostly dependent on the dielectric properties of the reflector (Larson et al., 2008a; Nievinski and Larson, 2014a). For cases when the reflecting material is not constant,  $\varphi$  can instead be implemented as a time dependent function. Finally, as the main usage of GNSS reflectometry in this thesis concerns the retrieval of sea surface height, which is continuously changing over time, the height will be implemented as a B-spline function. This will be described in more detail later in this chapter.

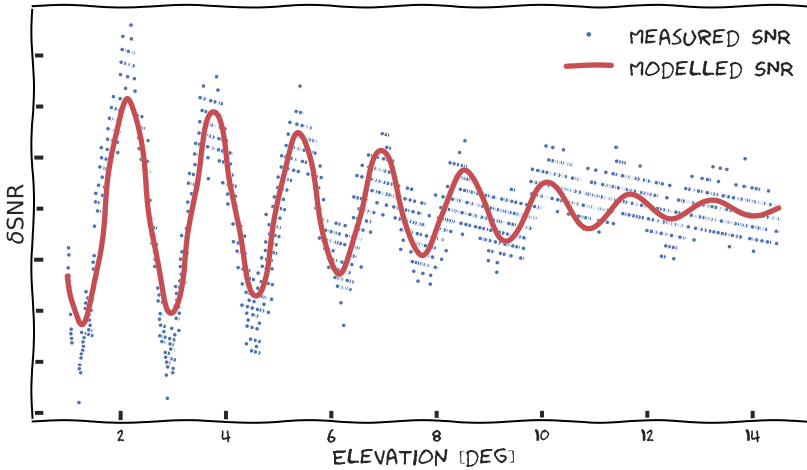


Figure 2.7: *Detrended signal-to-noise ratio measurements as well as the modelled values using Equation (2.14). The data used in the figure comes from the same satellite passage as the data in Figure 2.4.*

For numerical stability, the amplitude and phase will instead be implemented as the in-phase/out-of-phase components  $C_1$  and  $C_2$ . Also, instead of modelling  $s$ , the square will be used directly  $\gamma = s^2$ . This is also to stress that the values for damping do not directly correspond to the roughness, as the unmodeled antenna gain pattern will also affect the retrieved values. With these considerations, the inversion model of Equation (2.13) can be implemented as:

$$\delta\text{SNR} = \left( C_{i,1} \sin \left( \frac{4\pi(h - \delta h_i)}{\lambda_i} \sin \varepsilon \right) + C_{i,2} \cos \left( \frac{4\pi(h - \delta h_i)}{\lambda_i} \sin \varepsilon \right) \right) \times \exp(-4k_i^2 \gamma \sin^2 \varepsilon). \quad (2.14)$$

The offset  $\delta h$  is added as the phase centre of an antenna and its geometrical centre is not the same. The magnitude of  $\delta h$  depends on the frequency of the signal and is for most antennas a known quantity.

The variables in Equation (2.14) with  $i$  as a subscript denote quantities which are dependent on the satellite system and transmission frequency, i.e. for example the GPS L1 frequency and the GLONASS L2 frequency. These are variables that either have a physical difference between different frequencies, i.e.  $\lambda$  and  $k$ , or which are different by system design. The variables  $h$  and  $\gamma$ , which relate to geometrical properties of the surroundings of the GNSS receiver, are however independent of the GNSS system and frequency and can therefore be shared by all measurements.

The system independent variables, i.e. reflector height and the damping parameter, allow us to use all available satellite measurements at a given time to retrieve the reflector height, regardless of the source. Moreover, as the height is implemented as a function of time, it is possible to use data from a longer time

span in one inversion. In doing so we can use the knowledge that the sea surface height changes smoothly in order to stabilise the solutions. The time dependence of the function also implicitly solves the problem of  $\dot{h}$  described in Section 2.2.

### 2.3.1 Representing Height as Time Dependent B-spline

The possibility to use a time dependent reflector height is the main feature that distinguishes the inversion method from for example Lomb-Scargle analysis. Whereas the latter retrieves reflector heights for each individual satellite passage independently, the usage of some continuous function allows us to restrict the solution to physically reasonable height variations. For example, we know that the sea surface height changes smoothly, and that on many locations the change is bound to the tidal cycle with some typical time scales of the variation. If desired, such information can be included in the choice of parametrisation of the height function, or the function can be kept more general. Also, a time dependent  $h$  makes the method inherently correcting for the change in the  $\delta\text{SNR}$  oscillation frequency that occurs during a satellite passage. In contrast, Lomb-Scargle analysis needs to adjust for a non-static reflector height using correction terms, as described in the previous section.

Here we will use B-spline functions to represent the time varying reflector height. B-spline functions are constructed from zero-degree basis functions defined as

$$N_j^0(t) = \begin{cases} 1 & \text{if } t_j \leq t < t_{j+1} \\ 0 & \text{otherwise} \end{cases} . \quad (2.15)$$

B-spline basis functions of higher order  $r$  can be recursively computed by the relation

$$N_j^r(t) = \frac{t - t_j}{t_{j+r} - t_j} N_j^{r-1}(t) + \frac{t_{j+r+1} - t}{t_{j+r+1} - t_{j+1}} N_{j+1}^{r-1}(t). \quad (2.16)$$

With these basis functions sea-surface height variations can be represented as

$$h(t) = \sum_{j=0}^{n-1} h_j N_j^r(t), \quad (2.17)$$

where the node values  $h_0 \dots h_{n-1}$  are retrieved from the signal-to-noise ratio data through inverse modelling.

The time scale that can be resolved is decided only by the number – or rather the density – of the basis nodes. The order of the B-spline basis functions determines the degree to which the function is continuously derivable. For sea surface applications we only make the assumption that the change rate is continuous so that the height function is twice derivable, i.e. B-spline order  $r = 2$ .

An important feature of B-spline functions is that they are obtained as a linear combination of the basis functions and node values as denoted in Equation (2.17). Therefore it is straightforward to evaluate the continuous function at any given epoch while only dealing with a relatively small number of coefficients. Moreover,

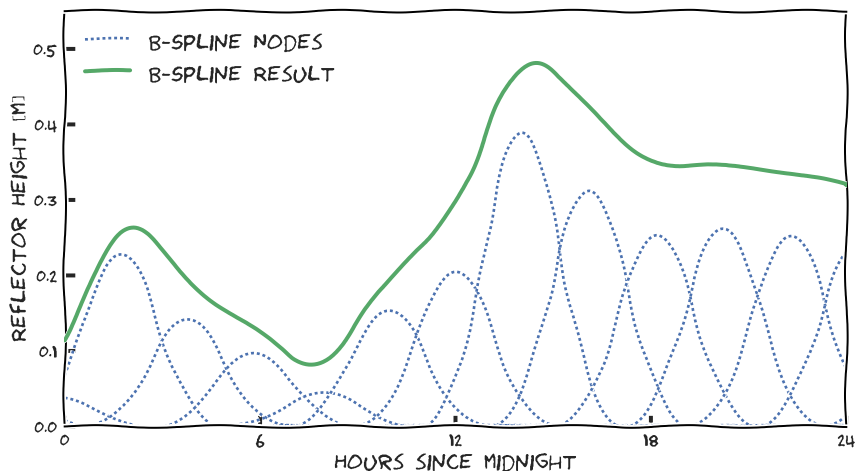


Figure 2.8: *Example of how B-splines can represent sea surface height by adding nodes with different scaling.*

the linearity of Equation (2.17) makes it easy to estimate the coefficients by least-squares methods. And as the model in Equation (2.14) already contains several non-linear functions, avoidance of unnecessary non-linearities is beneficial for the convergence of the inversion process.

### 2.3.2 Retrieval Procedure

To analyse the signal-to-noise ratio data it is important to understand which data is relevant for the inverse modelling. For most GNSS antennas there is only a limited view of the object of interest, for example the sea surface. Therefore, a sky mask is applied so that only measurements from directions in which water is known to exist are considered. Similar to the Lomb-Scargle analysis, before the signal-to-noise ratio data is analysed with inverse modelling the trend of the signal is removed using a low-order polynomial, since Equation (2.14) only describes the oscillating part of the measurements. Then, to retrieve the reflector height and other properties from the data, the model described by Equation (2.14) is fit to the measurements using least-squares adjustment. The parameters in the estimation process are  $[C_{1,1}, C_{1,2}, \dots, C_{m,1}, C_{m,2}, \gamma, h_0, \dots, h_{n-1}]$ , so the total number of parameters will be  $n + 2 \cdot m + 1$ , where  $m$  is the number of satellite systems in the analysis and  $n$  the number of B-spline nodes. As GNSS receivers generally have a sampling period of 30 s or less it is evident that the number of observations will greatly exceed the number of parameters, making the problem ideal for least-squares methods. However, the high non-linearity of the functional model in Equation (2.14) does not allow for a classical least-squares solution. Instead, an iterative non-linear

least-squares method needs to be applied, i.e. iteratively minimising

$$\sum_{i=1}^N |f(C_{1,1}, \dots, h_{n-1}) - \delta\text{SNR}|^2. \quad (2.18)$$

The MINPACK libraries (Moré et al., 1980), which are interfaced via the *optim* package within the Python framework SciPy (Millman and Aivazis, 2011; Oliphant, 2007), provide a convenient and easy-to-use environment which has been used in this work. Thus, inverse modeling of signal-to-noise ratio becomes possible even when the relation between the model parameters and the observed variations is highly non-linear.

As previously mentioned, a strength of the method is that measurements from different epochs and different GNSS systems can be used simultaneously. In principle, data from the whole analysis period can be analysed in a single inversion process. However, in order to make the dataset computationally feasible it is broken down into smaller pieces, and in our implementation we have chosen to use a single day as the basic unit. To avoid fitting problems at the day boundaries – which can happen if there is no data for a period around midnight – data from the two surrounding days are also used. With this procedure, using three days of data to compute one day of sea surface, we stabilise the B-spline solution and avoid problems at the edges.

## 2.4 Applications of GNSS Reflectometry

Up to this point, most of the examples given in the thesis refer to the retrieval of sea surface height, which have been the major focus in the development of the inversion algorithm. However, there are also other usages of GNSS reflectometry, such as snow height measurements, ice detection, and soil moisture measurements. Some of these are conceptually very similar to sea height retrievals, while others rely on other effects of the reflection. In this section a few usages will be described and the performance of inverse modelling will be analysed and compared to spectral analysis methods. The usages discussed will be sea level retrieval, ice detection, and snow height retrieval. Sea level retrieval and ice detection are also more extensively covered in the appended papers. GNSS-R has also been successfully used to measure soil moisture (Larson et al., 2008a) and vegetation biomass (Small et al., 2010). However, as these have so far not been tested with the inverse modelling, they will not be discussed further here.

### 2.4.1 Sea Surface Height Measurements

A primary focus of GNSS reflectometry is to determine the sea surface height. The long-term average sea surface height is naturally of interest for climate research, as it is expected that the sea level will change drastically within the next century in the context of global climate change. Accurate measurements of the sea surface height are also important for more applied usages: for maritime transportation

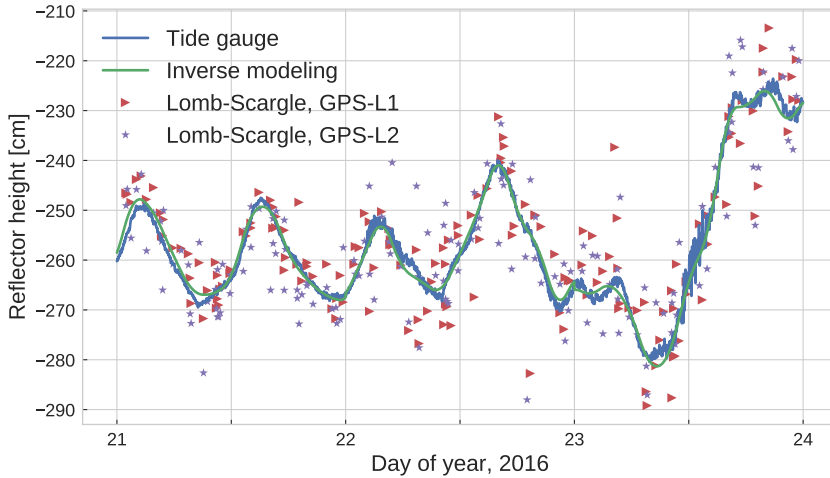


Figure 2.9: Comparison of tide gauge measurements and the two signal-to-noise ratio based GNSS reflectometry methods at GTGU, Onsala. The mean of each series is equalized to remove influences from different reference points.

planning it is important to know the navigable depth, and used at a dam the technique could provide information on the amount of water in a reservoir.

For sea surface measurements it is important to distinguish between apparent and real change. In some places around the world there is considerable post-glacial land uplift, on the order of centimetres per year (Johansson et al., 2002). If this is not taken into account properly it might appear that the sea surface is receding while it is in reality rising, just because the land is rising faster. Therefore, for long-term time series of the sea level it is important to consider the movement of the measurement apparatus. Traditional tide gauges only measure the sea surface height compared to a ground fixed measurement point, requiring another instrument to measure the absolute movement of the installation itself. GNSS reflectometry tide gauges, on the other hand, can measure their location with respect to the international terrestrial reference frame directly when determining the antenna position through GNSS positioning. Thus, it is possible to directly tie their sea level measurements to an absolute sea surface height. Another major benefit of using GNSS reflectometry for measuring sea surface is the price and ease of installation in comparison to for example a stilling well. This could potentially help in covering the parts of the world where tide gauge measurements are currently unavailable, or only very sparse, i.e. in the southern hemisphere.

The primary concern in using GNSS reflectometry is the precision. Earlier results from signal-to-noise ratio based GNSS reflectometry have shown differences to co-located tide gauges with a standard deviation of 4 cm to 6 cm on an ideal site with low tides and good view, depending on measurement period, and on the order of several decimetres for sites with larger tides (Löfgren and Haas, 2014;

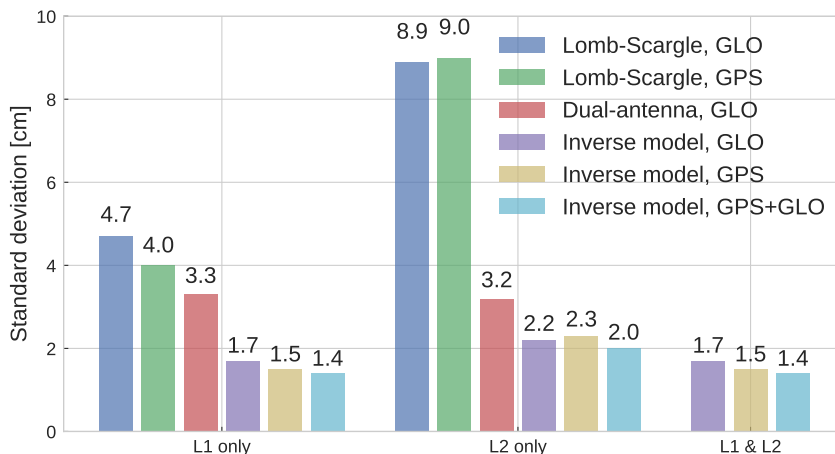


Figure 2.10: Comparison of the standard deviation of the difference from tide gauge data for different GNSS reflectometry methods and configurations at GTGU, Onsala. Data from a 30 day period between day number 273 to 303 of the year 2012. Results for Lomb-Scargle analysis and dual-antenna phase delay analysis come from Löfgren and Haas (2014).

Löfgren et al., 2014). Thus, a main objective in this thesis has been to increase the precision of the sea surface height retrieval. This is the topic of Paper I and Paper II.

In Figure 2.9 the tide gauge data is shown together with GNSS reflectometry results from both the Lomb-Scargle analysis as well as from the inverse modelling algorithm. From the figure it is clear that the inverse modelling follows the tide gauge data well, and even small features in the sea surface height time series are resolved, features which are not visible in the Lomb-Scargle data. This is even more evident from Figure 2.10, where the precision of different GNSS reflectometry algorithms are compared. The results in the figure show that inverse modelling can increase the precision drastically for signal-to-noise ratio methods, reducing the standard deviation from 4.0 cm to 1.4 cm at Onsala. As seen in Figure 2.10, the inverse algorithm even outperforms the dual-antenna method (see Section 2.1), which was previously the more precise method.

The stated accuracy of the reference measurements is 5 mm, and thus the uncertainty of the measurements are on the same order of magnitude. Together with the effect of averaging over longer time spans, this precision should allow GNSS reflectometry measurements to be usable for observations of changes to the mean sea level. Especially as GNSS reflectometry has the inherent capability to tie sea level measurements to the international terrestrial reference frame, accounting for any local land uplift.

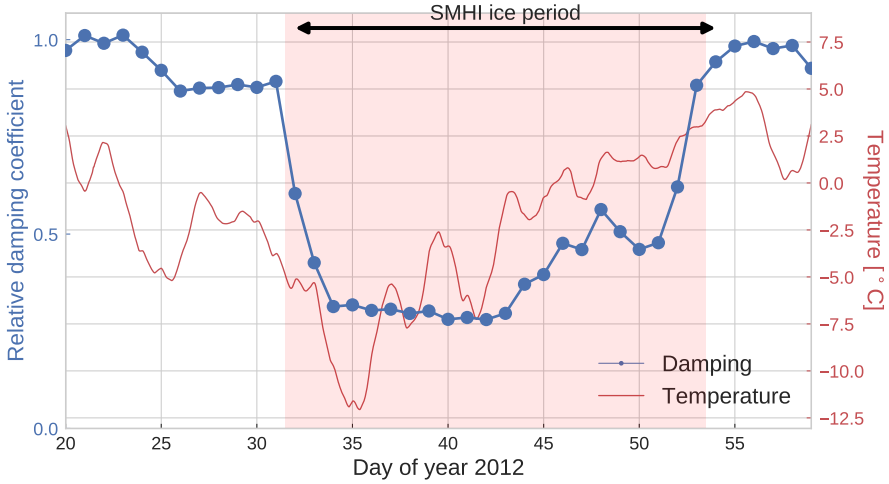


Figure 2.11: *Time series of damping values retrieved from the inverse modelling algorithm, from GTGU during the winter of 2012, normalised with the mean of a completely ice free period. The red line shows a one day moving average of the air temperature, and the shaded area represents the period during which SMHI ice maps show ice at Onsala.*

## 2.4.2 Ice Detection

During the retrieval process in the inverse modelling, more parameters than just reflector height are obtained. As explained in Section 2.3, these parameters also map to physical features of the reflecting surface. In this section we will focus on the damping parameter  $\gamma$  in Equation (2.14), which is affected by both dielectric and geometric properties of the reflector. As described in Paper III, the physical transition from water to ice affects exactly these properties, and thus the damping parameter.

In Figure 2.11 a time series of the retrieved damping values from the winter of 2012 is depicted. In the figure, temperature data and ice map data from the Swedish Meteorological and Hydrological Institute (SMHI) are also shown. During a completely ice free year, the normalised damping values stayed within the range 0.91 to 1.06. However, as seen in Figure 2.11, there is a significant drop in damping during the winter of 2012. The drop happens a few days after the temperature at the site has dropped below the the freezing temperature of sea water at the Swedish west coast, i.e.  $-1.4^{\circ}\text{C}$  (Fujino et al., 1974). It also coincides with the date when SMHI reports that ice formed on the sea in the area, marked by the red shade in the figure. The damping then stays low for the whole period during which the ice maps show ice coverage, returning to normal values only when the ice disappears.

The correlation between the damping value and the ice maps shows that the

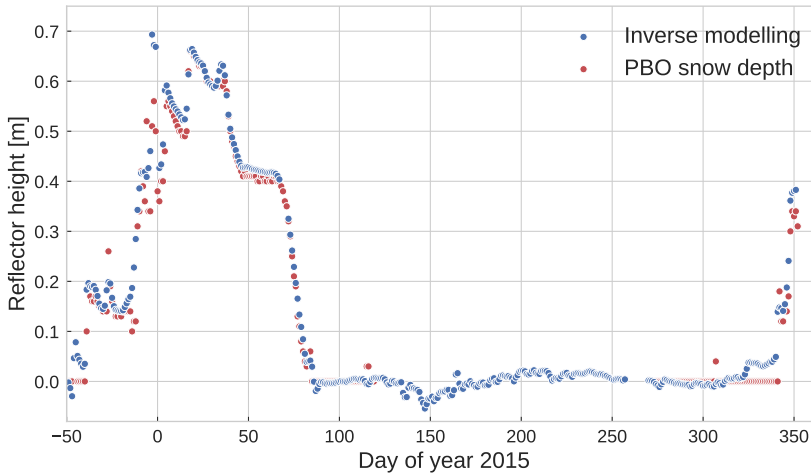


Figure 2.12: Comparison of snow level retrieval at the P360 GNSS installation through inverse modelling and the snow level reported by the GNSS-R based PBO network using Lomb-Scargle analysis (Larson and Nievinski, 2013). For the inverse modelling, the height is assumed to be constant for a retrieval cycle, as opposed to sea level measurements where B-splines are used.

damping value is an excellent indicator for local sea ice coverage around a GNSS installation. Therefore, a network of coastal GNSS stations in arctic and sub-arctic regions could be used to monitor coastal sea ice extent, a region in which satellite imaging often has too coarse resolution. This could provide valuable input data to climate studies as well as for more practical problems such as transportation planning.

### 2.4.3 Snow Depth Measurements

The snow cover constitutes an important part of the water cycle, storing water during the winter and being the primary water source in many parts of the world (Barnett et al., 2005). Therefore, it is important to study how the snow cover fluctuates with seasons, and how it changes over longer time scales. Many of the GNSS stations used for monitoring plate motion and land uplift are located in regions where snow fall occurs during the winter. Therefore, being able to use these as snow depth instruments gives access to a large set of automatically retrieved data (Larson and Small, 2016).

Measuring snow depth with GNSS reflectometry is conceptually very similar to measuring sea surface height. In both cases we are interested in the distance between the reflector and the antenna. In the snow measurement case, this can then be compared to the distance measured during the snow free season to deduce how much snow has fallen. The main difference between the two applications

is that snow does not experience tides and therefore we can use a much more slowly varying height function, as in Figure 2.12, where the snow height is retrieved once per day. However, one has to consider that snow depth can be directionally dependent as the snow cover can be affected by local topography and composition.

Figure 2.12 depicts a qualitative comparison of snow heights retrieved by inverse modelling and snow heights from the proven Lomb-Scargle based Plate boundary observatory (PBO) snow retrieval (Larson and Nievinski, 2013). It can be seen that the two time series mainly show the same behaviour, which proves that the inverse modelling can also be useful for snow height retrieval. The small variation in reflector height during summer is most likely due to vegetation variations. To further analyse and evaluate the performance, more comparisons to ground truth data are needed.



## Chapter 3

### Summary and Outlook

The work in this thesis and the appended papers focuses on improving the retrieval procedure in GNSS reflectometry. In the process we have found new measures of the signal-to-noise ratio pattern that can be used to detect the presence of sea ice. Continuing on this track we expect that there will be other analysis strategies yet to be discovered as more effects are accounted for in the inverse modelling procedure. To this end we will in the future focus on improving the method with for example accurate models of the antenna gain pattern and the combined effect with the Fresnel reflection coefficients. Other effects that will be of more importance when the precision of the retrieved values increases may include the elevation dependence of the antenna phase centre, which offsets the height measurements (Nievinski, 2013). Correct modelling of such effects would therefore increase the precision of the algorithm further.



## Chapter 4

### Summary of Appended Papers

This chapter briefly summarizes the main findings of the three papers upon which this thesis is based.

#### **4.1 Summary of Paper I: Inverse modelling of GNSS multipath for sea level measurements - initial results**

In a previous study by Nievinski and Larson (2014a) a model for forward modelling SNR measurements from multipath reflection was described. The model was then later successfully used for retrieving snow heights from SNR measurements (Nievinski and Larson, 2014b,c). However, on the relevant time scales, snow can mostly be considered as a static surface without any height change. Therefore, based on this forward model, we developed our own inversion algorithm for sea surface height retrievals where we fit a functional model of the SNR variations over elevations (see Section 2.3). In the model, the sea surface height is represented as a B-spline function, which makes the method intrinsically able to handle tides and other changes of sea surface height. In Paper I we introduce and test the model at the GNSS reflectometry test installation GTGU, situated at Onsala Space Observatory, Sweden.

#### **4.2 Summary of Paper II: Improving GNSS-R sea level determination through inverse modelling of SNR data**

In the second paper we extend the description and analysis of the inverse model. In Paper II, we also compare the performance of the inversion algorithm to the commonly used Lomb-Scargle spectral analysis on two coastal GNSS installations in Onsala, Sweden, and Spring Bay, Australia. We find that the new method has better precision having a standard deviation of 1.4 cm at Onsala and 2.9 cm at Spring Bay with respect to co-located tide gauges, less than half of the respective values for the Lomb-Scargle method. With wavelet analysis we also confirm that

the correlation between the tide gauge and the GNSS-R results are higher on all time scales for the inversion algorithm.

Finally, we conclude that the inversion algorithm also outperforms sea height retrievals based on the phase difference analysis. The phase difference method tends to fail in situations with high wind speed and in general performs poorly in terms of precision at moderate wind speeds.

With the increased precision and with their low maintenance needs, GNSS-R becomes a more feasible alternative to traditional tide gauges. Especially as there are already stations around the world that are close enough to the coast to be used directly, so called accidental tide gauges.

### **4.3 Summary of Paper III: Coastal sea ice detection using ground-based GNSS-R**

In Paper I and Paper II we explored fitting a functional model to data for retrieving sea surface height. However, height is not the only parameter in the fit. Therefore, in Paper III, we examine how other parameters of the inversion model couple to the physical parameters of the reflector. In particular we focus on winter periods during which sea ice is formed.

As described in Section 2.3, the dampening parameter in the model is sensitive to the roughness of the reflecting surface as well as the dielectric properties of the surface material. In the Paper III we notice that the damping parameter fluctuates around a stable value for most of the time. However, there are distinct periods where the damping drops by more than 60 %. Using GNSS data from the three winters of 2012, 2013, and 2016 together with temperature measurements and ice maps from SMHI we find that there is a strong correlation between the periods of low damping and the periods during which there is ice reported. Therefore, we conclude that the damping parameter is a good indicator for the presence of ice on the sea surface around a coastal GNSS-R installation. Finally, we also show that there are signs of the ice state in the estimated oscillation amplitude as well, although not as decisive as for the damping parameter.

## Bibliography

- Anderson, K. (2000). Determination of water level and tides using interferometric observations of GPS signals. *Journal of Atmospheric and Oceanic Technology*, **17**(8), 1118–1127. DOI: 10.1175/1520-0426(2000)017<1118:DOWLAT>2.0.CO;2.
- Barnett, T., J. Adam, and D. Lettenmaier (2005). Potential impacts of a warming climate on water availability in snow-dominated regions. *Nature*, **438**(7066), 303–309. DOI: 10.1038/nature04141.
- Beckmann, P. and A. Spizzichino (1987). *The scattering of electromagnetic waves from rough surfaces*. Artech House, Inc.
- Dow, J. M., R. Neilan, and C. Rizos (2009). The international GNSS service in a changing landscape of global navigation satellite systems. *Journal of Geodesy*, **83**(3-4), 191–198. DOI: 10.1007/s00190-008-0300-3.
- Fabra, F., E. Cardellach, A. Rius, S. Ribo, S. Oliveras, O. Nogues-Correig, M. B. Rivas, M. Semmling, and S. D’Addio (2012). Phase Altimetry With Dual Polarization GNSS-R Over Sea Ice. *IEEE Transactions on Geoscience and Remote Sensing*, **50**(6), 2112–2121. DOI: 10.1109/TGRS.2011.2172797.
- Fujino, K., E. Lewis, and R. Perkin (1974). The freezing point of seawater at pressures up to 100 bars. *Journal of Geophysical research*, **79**(12), 1792–1797.
- Garrison, J. L., S. J. Katzberg, and M. I. Hill (1998). Effect of sea roughness on bistatically scattered range coded signals from the Global Positioning System. *Geophysical Research Letters*, **25**(13), 2257–2260. DOI: 10.1029/98GL51615.
- Georgiadou, Y. and A. Kleusberg (1988). On carrier signal multipath effects in relative GPS positioning. *Manuscripta geodetica*, **13**(3), 172–179.
- Johansson, J. M., J. L. Davis, H. G. Scherneck, G. A. Milne, M. Vermeer, J. X. Mitrovica, R. A. Bennett, B. Jonsson, G. Elgered, P. Elósegui, H. Koivula, M. Poutanen, B. O. Rönnäng, and I. I. Shapiro (2002). Continuous GPS measurements of postglacial adjustment in Fennoscandia 1. Geodetic results. *Journal of Geophysical Research: Solid Earth*, **107**(B8). DOI: 10.1029/2001JB000400.

- Larson, K. M., R. D. Ray, F. G. Nievinski, and J. T. Freymueller (2013). The Accidental Tide Gauge: A GPS Reflection Case Study From Kachemak Bay, Alaska. *IEEE Geoscience and Remote Sensing Letters*, **10**(5), 1200–1204. DOI: 10.1109/LGRS.2012.2236075.
- Larson, K. M. and E. E. Small (2016). Estimation of Snow Depth Using L1 GPS Signal-to-Noise Ratio Data. *IEEE Journal of Selected Topics in Applied Earth Observations and Remote Sensing*, **9**(10), 4802–4808. DOI: 10.1109/JSTARS.2015.2508673.
- Larson, K. M. and F. G. Nievinski (2013). GPS snow sensing: results from the EarthScope Plate Boundary Observatory. *GPS Solutions*, **17**(1), 41–52. DOI: 10.1007/s10291-012-0259-7.
- Larson, K. M., E. E. Small, E. D. Gutmann, A. L. Bilich, J. J. Braun, and V. U. Zavorotny (2008a). Use of GPS receivers as a soil moisture network for water cycle studies. *Geophysical Research Letters*, **35**(24). L24405. DOI: 10.1029/2008GL036013.
- Larson, K. M., E. E. Small, E. Gutmann, A. Bilich, P. Axelrad, and J. Braun (2008b). Using GPS multipath to measure soil moisture fluctuations: initial results. *GPS Solutions*, **12**(3), 173–177. DOI: 10.1007/s10291-007-0076-6.
- Löfgren, J. S., R. Haas, H. G. Scherneck, and M. S. Bos (2011a). Three months of local sea level derived from reflected GNSS signals. *Radio Science*, **46**(6). DOI: 10.1029/2011RS004693.
- Löfgren, J. S. and R. Haas (2014). Sea level measurements using multi-frequency GPS and GLONASS observations. *EURASIP Journal on Advances in Signal Processing*, **2014**(1), 50. DOI: 10.1186/1687-6180-2014-50.
- Löfgren, J. S., R. Haas, and J. M. Johansson (2011b). Monitoring coastal sea level using reflected GNSS signals. *Advances in Space Research*, **47**(2). Scientific applications of Galileo and other Global Navigation Satellite Systems - I, 213–220. DOI: 10.1016/j.asr.2010.08.015.
- Löfgren, J. S., R. Haas, and H. G. Scherneck (2014). Sea level time series and ocean tide analysis from multipath signals at five {GPS} sites in different parts of the world. *Journal of Geodynamics*, **80**. SI: Understand the Earth, 66–80. DOI: 10.1016/j.jog.2014.02.012.
- Martin-Neira, M. (1993). A passive reflectometry and interferometry system (PARIS): Application to ocean altimetry. *ESA journal*, **17**, 331–355.
- Martin-Neira, M., M. Caparrini, J. Font-Rossello, S. Lannelongue, and C. S. Vallmitjana (2001). The PARIS concept: an experimental demonstration of sea surface altimetry using GPS reflected signals. *IEEE Transactions on Geoscience and Remote Sensing*, **39**(1), 142–150. DOI: 10.1109/36.898676.
- Martin-Neira, M., P. Colmenarejo, G. Ruffini, and C. Serra (2002). Altimetry precision of 1 cm over a pond using the wide-lane carrier phase of GPS reflected

- signals. *Canadian Journal of Remote Sensing*, **28**(3), 394–403. DOI: 10.5589/m02-039.
- Millman, K. J. and M. Aivazis (2011). Python for scientists and engineers. *Computing in Science & Engineering*, **13**(2), 9–12. DOI: 10.1109/MCSE.2011.36.
- Moreé, J. J., B. S. Garbow, and K. E. Hillstrom (1980). *User guide for MINPACK-1*. Tech. rep. CM-P00068642.
- Nievinski, F. G. and K. M. Larson (2014a). Forward modeling of GPS multipath for near-surface reflectometry and positioning applications. *GPS Solutions*, **18**(2), 309–322. DOI: 10.1007/s10291-013-0331-y.
- (2014b). Inverse Modeling of GPS Multipath for Snow Depth Estimation—Part I: Formulation and Simulations. *IEEE Transactions on Geoscience and Remote Sensing*, **52**(10), 6555–6563. DOI: 10.1109/TGRS.2013.2297681.
- (2014c). Inverse modeling of GPS multipath for snow depth estimation—Part II: application and validation. *IEEE Transactions on Geoscience and Remote Sensing*, **52**(10), 6564–6573. DOI: 10.1109/TGRS.2013.2297688.
- Nievinski, F. G. (2013). “Forward and inverse modeling of GPS multipath for snow monitoring”. PhD thesis. University of Colorado.
- Oliphant, T. E. (2007). Python for scientific computing. *Computing in Science & Engineering*, **9**(3). DOI: 10.1109/MCSE.2007.58.
- Small, E. E., K. M. Larson, and J. J. Braun (2010). Sensing vegetation growth with reflected GPS signals. *Geophysical Research Letters*, **37**(12). L12401. DOI: 10.1029/2010GL042951.
- Strandberg, J., T. Hobiger, and R. Haas (2016a). Improving GNSS-R sea level determination through inverse modeling of SNR data. *Radio Science*, **51**(8), 1286–1296. DOI: 10.1002/2016RS006057.
- (2016b). “Inverse modelling of GNSS multipath for sea level measurements - initial results”. *Proc. of International Geoscience and Remote Sensing Symposium 2016 (IGARSS 2016)*. DOI: 10.1109/IGARSS.2016.7729479.
- (2017). Coastal sea ice detection using ground-based GNSS-R. *IEEE Geoscience and Remote Sensing Letters*, in press.